An efficient kinetic modeling in plasmas relevant to inertial confinement fusion by using the AWBS transport equation

Authors*
Centre Lasers Intenses et Applications,
Universite de Bordeaux-CNRS-CEA,
UMR 5107, F-33405 Talence, France.
(Dated: July 11, 2018)

Text of abstract.

I. INTRODUCTION

The first attempts of modern kinetic modeling of plasma can be tracked back to the fifties, when Cohen, Spitzer, and Routly (CSR) [1] in detail demonstrated the fact, that in the ionized gas the effect of Coulomb collisions between electrons and ions predominantly results from frequently occurring events of cumulative small deflections rather than occasional close encounters. This effect was originally described by Jeans in [2] and Chandrasekhar [3] proposed to use the diffusion equation model of the Fokker-Planck type (FP) [4].

As a result, a classical paper by Spitzer and Harm (SH) [5] provides the computed electron distribution function spanning from low to high Z plasmas, and more importantly, the current and heat flux formulas, which are widely used in almost every plasma hydrodynamic code nowadays. The distribution function is of the form $f^0 + \mu f^1$, where f^0 and f^1 are isotropic and μ, is the direction cosine between the particle trajectory and some preferred direction in space. It should be emphasized that the SH solution expresses a small perturbation of equilibrium, i.e. that f^0 is the Maxwell-Boltzmann distribution and μf^1 represents a very small deviation.

The actual cornerstone of the modern FP simulations was set in place by Rosenbluth [6], when he derived a simplified form of the FP equation for a finite expansion of the distribution function, where all the terms are computed according to plasma conditions, including f^0, which of course needs to tend to the Maxwell-Boltzmann distribution.

Previously the VlasovFokkerPlanck (VFP) equation has been solved numerically ignoring magnetic fields in 1-D (1 spatial dimension) [7, 8] to address heatflow down steep temperature gradients in unmagnetised plasma. Under these conditions the classical, fluid description of transport [5, 9], which makes the local approximation, breaks down. They found that non-local effects are responsible for thermal transport inhibition [7].

Particle-in-cell (PIC) codes [10] are fully kinetic and are ideally suited to collisionless plasmas. Typically PIC codes tend to use explicit methods and consequently require a time step small enough to resolve the fastest frequency present in the problem. They also suffer from the so called "finite grid instability" [10] whereby the plasma numerically heats up until the electron debye length is resolved by the grid. These limitations mean that multidimensional, explicit, PIC cannot readily simulate the low temperature, high density plasma created in lasersolid interactions. One spatial dimension PIC codes with electronion collisions have successfully been applied to fast electron transport through solid density plasma [11, 12]. Explicit 2-D PIC is unable to access conditions where collisions dominate for the bulk of the electrons, though. Even though implicit methods overcome this particular problem, the PIC method in general struggles to adequately resolve the distribution function in a given cell when a realistic sized, 2-D problem is addressed. Statistical noise and under resolution of the electron distribution lead to an inaccurate treatment of collisions and can overwhelm real physical effects present.

In is the purpose of this paper to present an efficient alternative to FP model based on the Albritton-Williams-Bernstein-Swartz collision operator (AWBS) [13]. In Section II we propose a modified form of the AWBS collision operator, where its important properties are further presented in Section III with the emphasis on its comparison to the full FP solution in local diffusive regime. Section IV focuses on the performance of the AWBS transport equation model compared to modern kinetic codes including FP codes Aladin and Impact, and PIC code Calder, where the cases related to real laser generated plasma conditions are studied. Finally, the most important outcomes of our research are concluded in Section V.

II. THE AWBS KINETIC MODEL

The electrons in plasma can be modeled by the deterministic Vlasov model of charged particles

$$\frac{\partial f}{\partial t} + \boldsymbol{v} \cdot \nabla_{\boldsymbol{x}} f + \tilde{\boldsymbol{E}} \cdot \nabla_{\boldsymbol{v}} f = C_{ee}(f) + C_{ei}(f), \quad (1)$$

where $f(t, \boldsymbol{x}, \boldsymbol{v})$ represents the density function of electrons at time t, spatial point $\boldsymbol{x}$, and velocity $\boldsymbol{v}$, and $\tilde{\boldsymbol{E}} = \frac{q_e}{m_e}\boldsymbol{E}$ is the existing electric field in plasma.

The generally accepted form of the electron-electron collision operator C_{ee} is the Fokker-Planck form pub-

* milan.holec@u-bordeaux.fr

lished by Landau [14]

$$C_{FP}(f) = \Gamma \int \nabla_{\boldsymbol{v}} \nabla_{\boldsymbol{v}} (\boldsymbol{v} - \tilde{\boldsymbol{v}}) \cdot (f \nabla_{\tilde{\boldsymbol{v}}} f - f \nabla_{\boldsymbol{v}} f) \, \mathrm{d}\tilde{\boldsymbol{v}}, \quad (2)$$

where $\Gamma = \frac{q_e^4 \ln\Lambda}{4\pi\epsilon^2 m_e^2}$ and $\ln\Lambda$ is the Coulomb logarithm. In principal, the electron-ion collision operator C_{ei} could be expressed in the form similar to (2), but since ions are considered to be motionless compared to electrons, the scattering operator, i.e. no change in the velocity magnitude, expressed in spherical coordinates is widely accepted

$$C_{ei}(f) = \frac{\nu_{ei}}{2} \left(\frac{\partial}{\partial \mu} \left((1-\mu^2) \frac{\partial f}{\partial \mu} \right) + \frac{1}{\sin^2(\phi)} \frac{\partial^2 f}{\partial \theta^2} \right), \quad (3)$$

where $\mu = \cos(\phi)$, ϕ and θ are the polar and azimuthal angles, and $\nu_{ei} = \frac{Z n_e \Gamma}{v^3}$ is the electron-ion collision frequency.

Fish introduced an alternative form of C_{ee} in [15] referred to as high-velocity limit electron collision operator

$$C_H(f) = v\nu_e \frac{\partial}{\partial v} \left(f + \frac{v_{th}^2}{v} \frac{\partial f}{\partial v} \right) + \frac{\nu_e}{2} \left(1 - \frac{v_{th}^2}{2v^2} \right) \left(\frac{\partial}{\partial \mu} \left((1-\mu^2) \frac{\partial f}{\partial \mu} \right) + \frac{1}{\sin^2(\phi)} \frac{\partial^2 f}{\partial \theta^2} \right), \quad (4)$$

where $\nu_e = \frac{n_e \Gamma}{v^3}$ is the electron-electron collision frequency and $v_{th} = \sqrt{\frac{k_B T_e}{m_e}}$ is the electron thermal velocity. The linear form of C_H arises from an assumption that the fast electrons predominantly interact with the thermal (slow) electrons, which simplifies importantly the nonlinear form (2).

The aim of this work is to use a yet simpler form of the electron-electron collision operator, i.e. the AWBS formulation [13], where we propose the following form

$$C_{AWBS}(f) = v \frac{\nu_e}{2} \frac{\partial}{\partial v} (f - f_M) + \frac{\nu_{ei} + \frac{\nu_e}{2}}{2} \left(\frac{\partial}{\partial \mu} \left((1-\mu^2) \frac{\partial f}{\partial \mu} \right) + \frac{1}{\sin^2(\phi)} \frac{\partial^2 f}{\partial \theta^2} \right), \quad (5)$$

where f_M is the Maxwell-Boltzmann equilibrium distribution. C_{AWBS} represents the complete $C_{ee} + C_{ei}$ collision operator in (1).

The complete form of collision operator (5) was previously introduced in [16, 17], nevertheless, we intentionally use a half of the electron-electron collisional frequency modification $\frac{\nu_e}{2}$, because this formulation provides very promising results compared to the full FP operator as emphasized in Section III.

The Maxwell-Boltzmann averaged e-e scattering in (4) can be approximated as $\nu_e \int \left(1 - \frac{v_{th}^2}{2v^2}\right) f_M 4\pi v^2 \, \mathrm{d}v = \frac{\nu_e}{2}$.

III. BGK, AWBS, AND FOKKER-PLANCK MODELS IN LOCAL DIFFUSIVE REGIME

In a broad analysis of the electron transport, any qualitative information about its properties are highly welcome. Even better, if one can extract some qualitative information, which provides comparative and reliable results in a clear way, the confidence of using a transport model, e.g. (5), can lead to efficient yet relatively cheap computation cost predictions of real physics.

In this paper, we can try to find an approximate solution to the so-called *local diffusive regime* of electro transport, where the *diffusive regime*, in general, refers to a low anisotropy in angle given by μ, and *local* means that the mean free path of electrons λ_{ei} is rather restricted compared to the plasma spatial scale. In the words of mathematics this corresponds to the first order expansion in λ_{ei} and μ of the distribution function as

$$\tilde{f}(z, v, \mu) = f^0(z, v) + f^1(z, v) \lambda_{ei} \mu, \quad (6)$$

where z is the spatial coordinate along the axis z, v the magnitude of transport velocity, and $\lambda_{ei} = \frac{v}{\nu_{ei}} = \frac{v^4}{Z n_e \Gamma}$. In other words, one can say that by evaluating numerically $\tilde{f}$ in (6), we accept some error of the order $O(\lambda_{ei}^2) + O(\mu^2)$. The expansion in a small parameter λ_{ei} is also coherent with a time-steady approximation due to the relation between the mean free path and collision frequency, where the higher the collision frequency the more steady the solution.

In order to start, we express the time-steady left hand side of (1) in 1D and insert the approximation (6), which leads to

$$\mu \left(\frac{\partial \tilde{f}}{\partial z} + \frac{\tilde{E}_z}{v} \frac{\partial \tilde{f}}{\partial v} \right) + \frac{\tilde{E}_z (1-\mu^2)}{v^2} \frac{\partial \tilde{f}}{\partial \mu} = \mu \left(\frac{\partial f^0}{\partial z} + \frac{\tilde{E}_z}{v} \frac{\partial f^0}{\partial v} \right) + \frac{\tilde{E}_z \lambda_{ei}}{v^2} f^1 + O(\mu^2), \quad (7)$$

and is truncated for low anisotropy, i.e. with error $O(\mu^2)$.

A. The BGK local diffusive electron transport

Even though the BGK plasma collisional operator [18]

$$\frac{1}{v} C_{BGK}(\tilde{f}) = \frac{\tilde{f} - f_M}{\lambda_e} + \frac{1}{2\lambda_{ei}} \frac{\partial}{\partial \mu} (1-\mu^2) \frac{\partial \tilde{f}}{\partial \mu}, \quad (8)$$

where $\lambda_e = Z\lambda_{ei}$, is not actually used in our nonlocal transport simulations, we consider it useful to include this simplest form of the Boltzmann transport collision operator, because of two reasons: a) it can be treated analytically in the local diffusive regime; and b) it represents the so-called phenomenological collision operator by

explicitly using the Maxwell-Boltzmann equilibrium distribution f_M, which proves to be very useful in coupling of the nonlocal electron transport to hydrodynamics.

If one applies the action of the right hand side, i.e. of (8), on the approximation (6) and sets the result to be equal to the left hand side (7), the corresponding terms in μ are governed by the following equations

$$f^0 = f_M + \frac{\tilde{E}_z}{v^2} f^1 Z \lambda_{ei}^2, \tag{9}$$

$$f^1 = -\frac{Z}{Z+1}\left(\frac{\partial f^0}{\partial z} + \frac{\tilde{E}_z}{v}\frac{\partial f^0}{\partial v}\right), \tag{10}$$

i.e. $f^0 = f_M + O(\lambda_{ei}^2)$ and $f^1 = -\frac{Z}{Z+1}\left(\frac{\partial f_M}{\partial z} + \frac{\tilde{E}_z}{v}\frac{\partial f_M}{\partial v}\right)$. Now the electric current expressing the contribution of every electron naturally tends to zero, i.e. the *quasi-neutrality* constraint, which lead to an analytic formula of the self-consistent electric field

$$\boldsymbol{j} \equiv q_e \int \boldsymbol{v}\tilde{f}\,\mathrm{d}\boldsymbol{v} = \boldsymbol{0} \rightarrow \tilde{\boldsymbol{E}} = v_{th}^2\left(\frac{\nabla\rho}{\rho} + \frac{5}{2}\frac{\nabla T}{T}\right). \tag{11}$$

Consequently, based on (9), (10), and (11), the analytic formula (6) of the electron distribution function reads

$$\tilde{f} = f_M - \frac{Z}{Z+1}\left(\frac{v^2}{2v_{th}^2} - 4\right)\frac{1}{T}\frac{\partial T}{\partial z} f_M \lambda_{ei}\mu, \tag{12}$$

which is nothing else than the famous Lorentz electron-ion collision gas model [19] scaled by a constant depending on Z, naturally arising from the BGK model (8).

B. The AWBS local diffusive electron transport

The main object of this work presented in Sec II simplifies in 1D to a relatively simple form of the Boltzmann transport collision operator (compared to (2))

$$\frac{1}{v}C_{AWBS}(f) = \frac{v}{2\lambda_e}\frac{\partial}{\partial v}(f - f_M) + \frac{1}{2}\left(\frac{1}{\lambda_{ei}} + \frac{1}{2\lambda_e}\right)\frac{\partial}{\partial\mu}(1-\mu^2)\frac{\partial f}{\partial\mu}. \tag{13}$$

Similarly to the BGK model, AWBS 13 is also referred to as a phenomenological model, since it explicitly uses the Maxwell-Boltzmann equilibrium distribution f_M, and also, makes it a very attractive model of the nonlocal electron transport to be coupled to hydrodynamics via the plasma electron temperature and density.

A qualitative information about the AWBS model is obtained while repeating the action on (6) by the left hand side (7) and by the right hand side (13) and setting the equality. The corresponding terms in μ are then governed by the following equations

$$\frac{\partial}{\partial v}\left(f^0 - f_M\right) = \frac{\tilde{E}_z}{v^3} f^1 2Z\lambda_{ei}^2, \tag{14}$$

$$\frac{v}{2Z\lambda_{ei}}\frac{\partial\left(f^1\lambda_{ei}\right)}{\partial v} - \frac{2Z+1}{2Z}f^1 = \frac{\partial f^0}{\partial z} + \frac{\tilde{E}_z}{v}\frac{\partial f^0}{\partial v}, \tag{15}$$

i.e. $f^0 = f_M + O(\lambda_{ei}^2)$, however, the f^1 does not have a straightforward analytic formula. In reality, f^1 arises from the ordinary differential equation (by inserting f_M into (15))

$$\frac{\partial f^1}{\partial v} + \frac{1}{v}(3-2Z)f^1 = \frac{2Z}{v}\left(\frac{1}{\rho}\frac{\partial\rho}{\partial z} + \left(\frac{v^2}{2v_{th}^2} - \frac{3}{2}\right)\frac{1}{T}\frac{\partial T}{\partial z} - \frac{\tilde{E}_z}{v_{th}^2}\right) f_M. \tag{16}$$

We will stick with a numerical solution of (16), where the details about the resulting distribution function can be found in Section III D.

C. The Fokker-Planck local diffusive electron transport

The Fokker-Plank (2) collision operator can be also written as [20]

$$\frac{1}{v}C_{FP}(f) = \frac{\Gamma}{v}\left(4\pi f^2 + \frac{\nabla_{\boldsymbol{v}}\nabla_{\boldsymbol{v}} f : \nabla_{\boldsymbol{v}}\nabla_{\boldsymbol{v}} g}{2}\right), \tag{17}$$

where $g(\boldsymbol{v}) = \int |\boldsymbol{v}-\tilde{\boldsymbol{v}}| f(\tilde{\boldsymbol{v}})\,\mathrm{d}\tilde{\boldsymbol{v}}$ is the Rosenbluth potential [6]. Since we are interested in the approximate solution in the local diffusive regime, it is convenient to use a low anisotropy approximation $\tilde{g} = g^0(f^0) + g^1(f^1)\lambda_{ei}\mu$, which arises based on Eq. 45 of [6].

For a better clarity we present the action of (17) in 1D

$$C_{FP}(\tilde{f}) = \Gamma\left(4\pi {f^0}^2 + \frac{1}{2}\frac{\partial^2 f^0}{\partial v^2}\frac{\partial^2 g^0}{\partial v^2} + \frac{1}{v^2}\frac{\partial f^0}{\partial v}\frac{\partial g^0}{\partial v}\right) + \frac{\mu}{Zn_e}\left[8\pi f^0 f^1 v^4 - v\left(\frac{\partial f^0}{\partial v}g^1 + \frac{\partial g^0}{\partial v}f^1\right) + \frac{1}{v^2}\left(\frac{\partial f^0}{\partial v}\frac{\partial(g^1 v^4)}{\partial v} + \frac{\partial g^0}{\partial v}\frac{\partial(f^1 v^4)}{\partial v}\right) + \frac{1}{2}\left(\frac{\partial^2 f^0}{\partial v^2}\frac{\partial^2(g^1 v^4)}{\partial v^2} + \frac{\partial^2 g^0}{\partial v^2}\frac{\partial^2(f^1 v^4)}{\partial v^2}\right)\right] + O(\lambda_{ei}^2, \mu^2), \tag{18}$$

truncated by the quadratic terms in the angular anisotropy and the transport localization.

If once more repeated the action on (6) by the left hand side (7) and by the right hand side (17) and setting the equality, the equation governing f^0 corresponding to μ^0 takes the form

$$4\pi {f^0}^2 + \frac{1}{2}\frac{\partial^2 f^0}{\partial v^2}\frac{\partial^2 g^0}{\partial v^2} + \frac{1}{v^2}\frac{\partial f^0}{\partial v}\frac{\partial g^0}{\partial v} = \frac{\tilde{E}_z}{v^5} f^1 Z n_e \lambda_{ei}^2 - \frac{2}{v^2}\left(\frac{\partial f^1\lambda_{ei}}{\partial v} - \frac{f^1\lambda_{ei}}{v}\right)\left(\frac{\partial g^1\lambda_{ei}}{\partial v} - \frac{g^1\lambda_{ei}}{v}\right), \tag{19}$$

where the fundamental property of the Fokker-Planck collision operator tending to the Maxwell-Boltzmann distribution f_M [21], leads to $f^0 = f_M + O(\lambda_{ei}^2)$, where

we write an explicit form of the quadratic term $O(\lambda_{ei}^2)$ obtained from the truncation (18). The equality corresponding to μ takes the form

$$\frac{1}{Zn_e}\left[\frac{1}{2}\left(\frac{\partial^2 f_M}{\partial v^2}\frac{\partial^2(g^1v^4)}{\partial v^2}+\frac{\partial^2 g_M}{\partial v^2}\frac{\partial^2(f^1v^4)}{\partial v^2}\right)+\frac{1}{v^2}\left(\frac{\partial f_M}{\partial v}\frac{\partial(g^1v^4)}{\partial v}+\frac{\partial g_M}{\partial v}\frac{\partial(f^1v^4)}{\partial v}\right)-v\left(\frac{\partial f_M}{\partial v}g^1+\frac{\partial g_M}{\partial v}f^1\right)+8\pi f_M f^1 v^4\right]-vf^1 = v\frac{\partial f_M}{\partial z}+\tilde{E}_z\frac{\partial f_M}{\partial v}, \quad (20)$$

which is the equation governing the unknown f^1.

In principle, the solution to the equation (20) is very ambitious, as demonstrated in [1, 3, 6], fortunately, one can use the explicit evaluation of the electron distribution function published in [5], which takes the following form

$$f^1(z,v)=\frac{1}{\lambda_{ei}}\frac{m_e^2}{4\pi q_e^4 \ln\Lambda}\frac{v_{2th}^4}{Z}\left(2d_T(v/v_{2th})+\frac{3}{2}\frac{\gamma_T}{\gamma_E}d_E(v/v_{2th})\right)\frac{f_M}{n_e}\frac{1}{T}\frac{\partial T_e}{\partial z}, \quad (21)$$

where $d_T(x)=ZD_T(x)/B$, $d_E(x)=ZD_E(x)/A$, γ_T, and γ_E are represented by numerical values in TABLE I, TABLE II, and TABLE III in [5], and $v_{2th}=\sqrt{\frac{k_B T_e}{2m_e}}$.

D. Summary of the BGK, AWBS, and Fokker-Planck local diffusive transport

Ever since the SH paper [5], the effect of microscopic electron transport on the current $\int q_e \boldsymbol{v}\tilde{f}\,\mathrm{d}\boldsymbol{v}$ and the heat flux $\int \frac{m_e|\boldsymbol{v}|^2}{2}\boldsymbol{v}\tilde{f}\,\mathrm{d}\boldsymbol{v}$ in plasmas under local diffusive conditions has been understood. By overcoming some delicate aspects of the numerical solution to (20) presented in the CSR paper [1], the effect of electron-electron collisions was properly quantified and the correct dependence on Z of the heat flux $\boldsymbol{q}$ was approximated as [22]

$$\boldsymbol{q}=\frac{Z+0.24}{Z+4.2}\boldsymbol{q}_L, \quad (22)$$

where $\boldsymbol{q}_L=\kappa T_e^{\frac{5}{2}}\nabla T_e$ is the heat flux given by Lorentz [19]. In order to follow the SH Z-dependence of heat flux, the BGK operator needs to be scaled as

$$\frac{Z+4.2}{Z+0.24}\frac{Z}{Z+1}\left[\nu_e\left(\tilde{f}-f_M\right)+\frac{\nu_{ei}}{2}\frac{\partial}{\partial\mu}(1-\mu^2)\frac{\partial\tilde{f}}{\partial\mu}\right],$$

which leads to a scaled Lorentz* distribution function

$$\tilde{f}=f_M-\frac{Z+0.24}{Z+4.2}\left(\frac{v^2}{2v_{th}^2}-4\right)\frac{1}{T}\frac{\partial T}{\partial z}f_M\lambda_{ei}\mu, \quad (23)$$

	$Z=1$	$Z=2$	$Z=4$	$Z=16$	$Z=116$
$\bar{\Delta}\boldsymbol{q}_{AWBS}$	0.057	0.004	0.038	0.049	0.004

TABLE I. Relative error $\bar{\Delta}\boldsymbol{q}_{AWBS}=|\boldsymbol{q}_{AWBS}-\boldsymbol{q}_{SH}|/\boldsymbol{q}_{SH}$ of the $\frac{\nu_e}{2}$ AWBS kinetic model equation (5) showing the discrepancy (maximum around 5%) with respect to the original solution of the heat flux given by numerical solution in Spitzer and Harm [5].

which obeys the Z-dependence (22).

On the contrary, the modified form of the AWBS collision operator (5) provides a very precise heat flux Z-dependence without introducing any scaling. Indeed, TABLE I shows the relative error (maximum around 5%) of the heat flux modeled by (5) vs. SH results represented by (22). It should be noted that the error is calculated with respect to original values presented in TABLE III in [5].

Nevertheless, the electron-electron collisions effect represented by (22) provides only an integrated information about the heat flux magnitude. If one takes a closure look at the distribution function itself, the conformity of the modified AWBS collision operator is even more emphasize as can be seen in FIG. 1 showing the flux moment in spherical coordinates of velocity

$$q_1=\frac{m_e v^2}{2}v f_1 v^2,$$

where f_1 is the anisotropic part of the distribution function, i.e. $f_1=f^1\lambda_{ei}$ ($\mu=1$) in the local diffusive transport.

In the case of the high Z Livermorium plasma ($Z=116$), AWBS exactly aligns with the Lorentz gas limit. In the opposite case of the low Z Hydrogen plasma ($Z=1$), the AWBS distribution function approaches significantly the numerical SH solution. Overall BGK behavior is consistent with the scaled Lorentz* distribution function (23) for any Z.

If one observes the f^1 equations of each of the model, i.e. (10), (16), and (20), it turns out to be clear that the terms containing derivatives with respect to v address important physical mechanisms of electron-electron collisions in plasma. In other words, even a simple linear first derivative term in the modified AWBS collision operator (5) (red dashed line) provides a significant model improvement with respect to the SH (Fokker-Planck) solution (solid black line) and compared to the simplest BGK model (dashed-dot blue line) in FIG. 1.

At last, we provide a qualitative information with respect to the dominant velocity of electrons contributing to the heat flux. In the high Z case all the models give $3.7\times v_{th}$, while SH solution gives $3.5\times v_{th}$ and

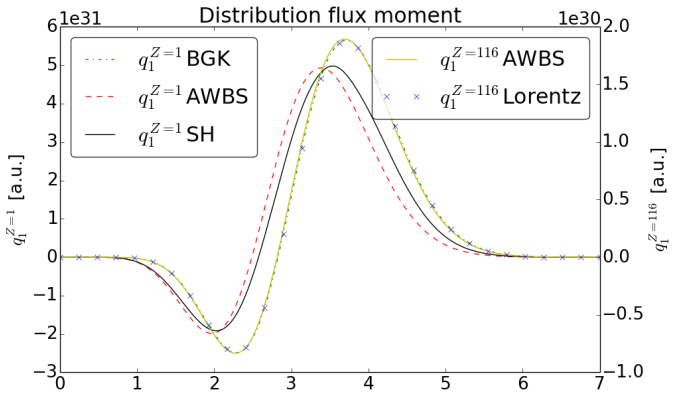

FIG. 1. The flux velocity moment of the anisotropic part of the electron distribution function in low $Z = 1$ and high $Z = 116$ plasmas in diffusive regime.

AWBS $3.4\times v_{th}$ in the case of low Z plasmas, thus showing the right tendency of the maximum velocity shift modeled by the modified AWBS collision operator (5).

IV. BENCHMARKING THE AWBS NONLOCAL TRANSPORT MODEL

After having shown several encouraging properties of the AWBS transport equation defined by (5) under local diffusive conditions in Sec. III, this section provides a broader analysis of the electron transport and focuses on analysis its behavior under variety of conditions in plasmas. In principle, this is characterized by allowing that electron mean free path can be arbitrarily long, which leads to so-called nonlocal electron transport extensively investigated in numerous publications [7, 16, 23–27], where the Fokker-Planck modeling of electrons in plasma represents the essential tool. Being so, we introduce our implementation of the AWBS transport equation called AP1, where its results are further benchmarked against simulation results provided by Aladin, Impact FP codes, and Calder a collisional Particle-In-Cell code. Their description follows in the next section.

A. AP1 implementation

AP1 represents the abbreviation AWBS-P1, i.e. the use of collision operator (5) and the P1 angular discretization, i.e. the lowest order anisotropy approximation. AP1 in general belongs to the so-called angular moments method and the electron distribution function takes the form

$$\tilde{f} = \frac{f_0}{4\pi} + \frac{3}{4\pi}\boldsymbol{n}\cdot\boldsymbol{f_1},$$

which consists of the isotropic part $f_0 = \int_{4\pi}\tilde{f}\mathrm{d}\boldsymbol{n}$ and the directional part $\boldsymbol{f_1} = \int_{4\pi}\boldsymbol{n}\tilde{f}\mathrm{d}\boldsymbol{n}$, where $\boldsymbol{n}$ is the transport direction (the solid angle).

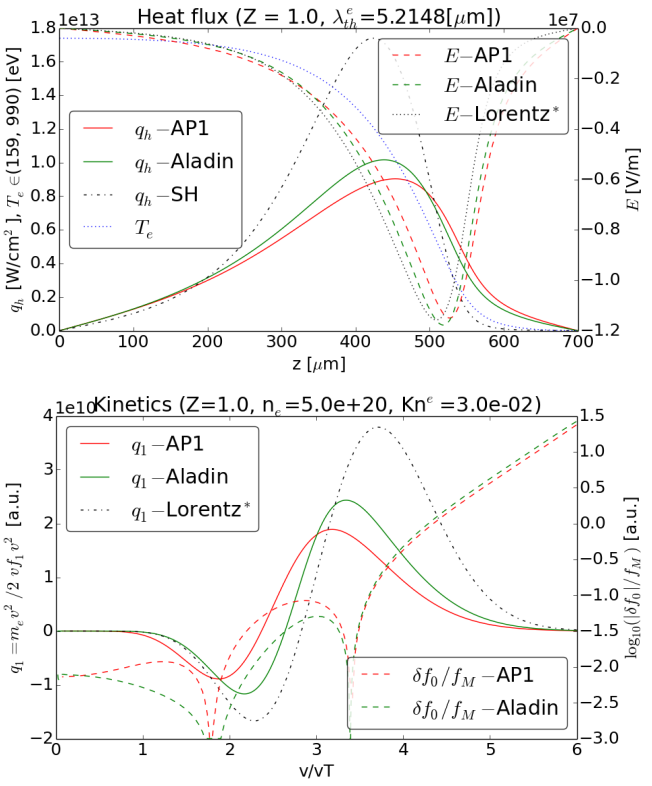

FIG. 2. Snapshot 20 ps. Left: correct steady solution of heat flux. Right: Aladins results are correct. Velocity limit 4.4 v_{th}..

The first two angular moments applied to the steady form of (1) with collision operator (5) lead to the AP1 model equations

$$v\frac{\nu_e}{2}\frac{\partial}{\partial v}\left(f_0 - 4\pi f_M\right) = v\nabla\cdot\boldsymbol{f_1} + \tilde{\boldsymbol{E}}\cdot\frac{\partial\boldsymbol{f_1}}{\partial v} + \frac{2}{v}\tilde{\boldsymbol{E}}\cdot\boldsymbol{f_1}, \quad (24)$$

$$v\frac{\nu_e}{2}\frac{\partial\boldsymbol{f_1}}{\partial v} - \nu_{scat}\boldsymbol{f_1} = \frac{v}{3}\nabla f_0 + \frac{\tilde{\boldsymbol{E}}}{3}\frac{\partial f_0}{\partial v}, \quad (25)$$

where $\nu_{scat} = \nu_{ei} + \frac{\nu_e}{2}$. The strategy of solving (24) and (25) resides in integrating $\frac{\partial f_0}{\partial v}$ and $\frac{\partial\boldsymbol{f_1}}{\partial v}$ in velocity magnitude while starting the integration from infinite velocity to zero velocity, which corresponds to decelerating electrons. It should be noted, that in practice we start the integration from $v = 7v_{th}$, which represents a sufficiently high velocity.

1. *Nonlocal electric field treatment*

Similarly to (11), one can obtain the model equation of the electric field $\tilde{\boldsymbol{E}}$ by evaluating the zero current con-

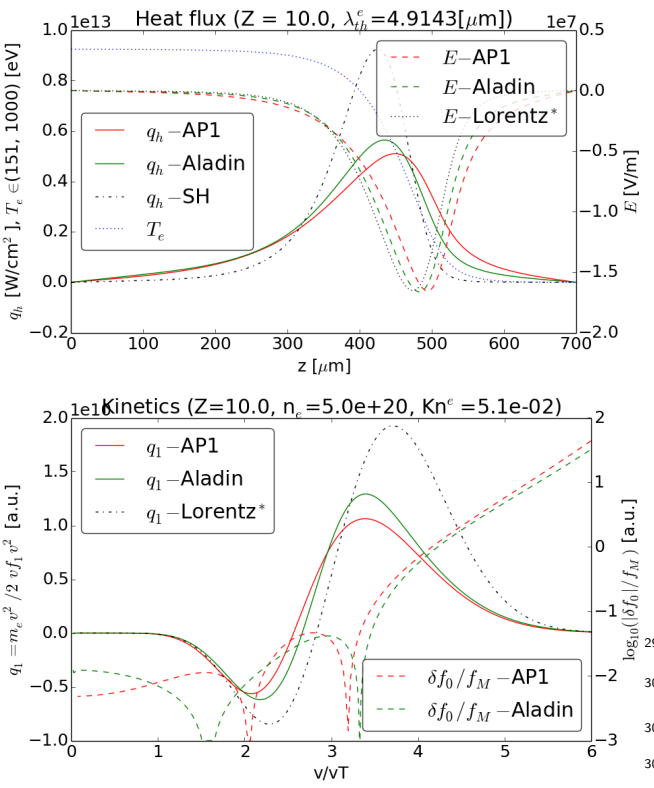

FIG. 3. Snapshot 12 ps. Left: correct steady solution of heat flux. Right: correct comparison to kinetic profiles at point 442 μm by Aladin. Velocity limit 3.4 v_{th}.

dition (a velocity integration of (25))

$$\int_v \left(\frac{\nu_e}{2} v^2 \frac{\partial \boldsymbol{f_1}}{\partial v} - \frac{v^2}{3\nu_{scat}} \nabla f_0 - \frac{v}{3\nu_{scat}} \frac{\partial f_0}{\partial v} \tilde{\boldsymbol{E}} \right) v^2 \, \mathrm{d}v = 0, \tag{26}$$

from which it is easy to express $\tilde{\boldsymbol{E}}$ once f_0 and $\boldsymbol{f_1}$ are known, or in other words, the integral-differential model equations need to be solved simultaneously, which is achieved by k-iteration of $f_0^k(\tilde{\boldsymbol{E}}^k)$, $\boldsymbol{f_1}^k(\tilde{\boldsymbol{E}}^k)$, i.e. (24), (25), and $\tilde{\boldsymbol{E}}^{k+1}(f_0^k, \boldsymbol{f_1}^k)$, i.e. (26), until the current evaluation (26) converges to zero. In principle, our concept of k-iteration resembles to the embedded nonlinear iteration of the implicit E field introduced in [28]. The first iteration starts with $\tilde{\boldsymbol{E}} = \boldsymbol{0}$ in (24) and (25) and usually less than 10 iterations is sufficient to obey the quasi-neutrality constraint.

Interestingly, we have encountered a very specific property of the AP1 model with respect to the electric field magnitude. The easiest way how to demonstrate this is to write the model equations (24) and (25) in 1D and eliminate one of the partial derivatives with respect to v. In the case of elimination of $\frac{\partial f_0}{\partial v}$ one obtains the following

Kn^e	10^{-4}	10^{-3}	10^{-2}	10^{-1}	1
v_{lim}/v_{th}	70.8	22.4	7.3	3.1	1.8

TABLE II. $\sqrt{3} v \frac{\nu_e}{2} > |\tilde{\boldsymbol{E}}|$.

equation

$$\left(v\frac{\nu_e}{2} - \frac{2\tilde{E}_z^2}{3v\nu_e} \right) \frac{\partial f_{1_z}}{\partial v} = \frac{2\tilde{E}_z}{3\nu_e} \frac{\partial f_{1_z}}{\partial z} + \frac{4\pi\tilde{E}_z}{3} \frac{\partial f_M}{\partial v} + \frac{v}{3} \frac{\partial f_0}{\partial z} + \left(\frac{4\tilde{E}_z^2}{3v^2\nu_e} + \left(\nu_{ei} + \frac{\nu_e}{2} \right) \right) f_{1_z}. \tag{27}$$

It is convenient to write the left hand side of (27) as $\frac{2}{3v\nu_e} \left(\left(\sqrt{3} v \frac{\nu_e}{2} \right)^2 - \tilde{E}_z^2 \right)$ from where it is clear that the bracket is negative if $\sqrt{3} v \frac{\nu_e}{2} = \sqrt{3} \frac{n_e \Gamma}{2v^2} < |\tilde{\boldsymbol{E}}|$, i.e. there is a velocity limit for a given magnitude $|\tilde{\boldsymbol{E}}|$, when the collisions are no more fully dominant and the electric field introduces a comparable effect to friction in the electron transport.

Since the last term on the right hand side of (27) is dominant, the solution behaves as $\boldsymbol{f_1} \sim \exp\left(- \left(\frac{4\tilde{E}_z^2}{3v^2\nu_e} + \left(\nu_{ei} + \frac{\nu_e}{2} \right) \right) / \left(v\frac{\nu_e}{2} - \frac{2\tilde{E}_z^2}{3v\nu_e} \right) v \right)$, which becomes ill-posed for velocities above the limit.

In order to provide a stable model, we introduce a reduced electric field

$$|\tilde{\boldsymbol{E}}_{red}| = \sqrt{3} v \frac{\nu_e}{2}, \tag{28}$$

ensuring that the bracket on the left hand side of (27) remains positive. Further more we define two quantities

$$\omega_{red} = \frac{|\tilde{\boldsymbol{E}}_{red}|}{|\tilde{\boldsymbol{E}}|}, \quad \nu_{scat}^E = \frac{|\tilde{\boldsymbol{E}}| - |\tilde{\boldsymbol{E}}_{red}|}{v}.$$

introducing the reduction factor of the electric field ω_{red} and the compensation of the electric field effect in terms of scattering ν_{scat}^E. Consequently, the AP1 model (24), (25), and (26) can be formulated as well posed with the help of ω_{red} and ν_{scat}^E. However, before doing so, we introduce a slightly different approximation to the electron distribution function as

$$\tilde{f} = \frac{4\pi f_M + \delta f_0}{4\pi} + \frac{3}{4\pi} \boldsymbol{n} \cdot \boldsymbol{f_1}. \tag{29}$$

where δf_0 represents the departure of isotropic part from the Maxwell-Boltzmann equilibrium distribution

f_M. Then, the stable AP1 model reads

$$v\frac{\nu_e}{2}\frac{\partial \delta f_0}{\partial v} = v\nabla\cdot\boldsymbol{f_1} + \tilde{\boldsymbol{E}}\cdot\left(\omega_{red}\frac{\partial \boldsymbol{f_1}}{\partial v} + \frac{2}{v}\boldsymbol{f_1}\right), \quad (30)$$

$$v\frac{\nu_e}{2}\frac{\partial \boldsymbol{f_1}}{\partial v} = \tilde{\nu}_{scat}\boldsymbol{f_1} + \frac{v}{3}\nabla\left(4\pi f_M + \delta f_0\right) + \frac{\tilde{\boldsymbol{E}}}{3}\left(4\pi\frac{\partial f_M}{\partial v} + \omega_{red}\frac{\partial \delta f_0}{\partial v}\right), \quad (31)$$

where $\tilde{\nu}_{scat} = \nu_{ei} + \nu^E_{scat} + \frac{\nu_e}{2}$. The reason for keeping f_M in the distribution function approximation (29) can be seen in the last term on the right hand side of (31), which provides the effect of electric field on directional quantities as current or heat flux. In principle, the explicit use of f_M ensures the proper effect of $\tilde{\boldsymbol{E}}$ if $\delta f_0 \ll f_M$, i.e. no matter what the reduction ω_{red} is. Apart from its stability, it also exhibits much better convergence of the electric field, which is now given by the zero current condition of (31) as

$$\tilde{\boldsymbol{E}} = \frac{\int_v \left(\frac{\nu_e}{2\tilde{\nu}_{scat}}v^2\frac{\partial \boldsymbol{f_1}}{\partial v} - \frac{v^2}{3\tilde{\nu}_{scat}}\nabla\left(4\pi f_M + \delta f_0\right)\right)v^2\,\mathrm{d}v}{\int_v \frac{v}{3\tilde{\nu}_{scat}}\left(4\pi\frac{\partial f_M}{\partial v} + \omega_{red}\frac{\partial \delta f_0}{\partial v}\right)v^2\,\mathrm{d}v}. \quad (32)$$

For practical reasons we present in TABLE II some explicit values of velocity limit corresponding to varying transport conditions expressed in terms of Knudsen number $\mathrm{Kn}^e = \frac{\lambda_e|\nabla T_e|}{T_e}$, where $\frac{T_e}{|\nabla T_e|}$ stands for the length scale of plasma.

B. Aladin, Impact, and Calder kinetic codes

- Brief description of the Aladin code FIG. 2, FIG. 3.
- Brief description of the Impact code FIG. 4.
- Brief description of the Calder code FIG. 5.

C. Large temperature variations tests

Among a variety of test suitable for benchmarking the nonlocal electron transport models published [16, 17, 22, 29–31], we decided to focus on conditions relevant to inertial confinement fusion plasmas generated by lasers.

1. *Heat-bath problem*

The first test case is a simple non-linear heat-bath problem, in which the initial temperature is $\tanh(z)$. The total computational box size is 700 μm in the case of Aladin and Impact and 1000 μm in the case of Calder. The Knudsen number has been varied to address a broad range of nonlocality of the electron transport corresponding to the laser-heated plasma conditions, i.e. $\mathrm{Kn}^e \in (0.0001, 1)$. The variation of Kn^e arises from the variation of the electron density $n_e \in (10^{19}, 10^{23})$ cm^{-3} or the slope of the temperature profile $s \in (25, 2500)\mu$m. The coulomb logarithm was held fixed throughout, $\ln\Lambda = 7.09$.

We now investigate the accuracy of the AP1, Aladin,

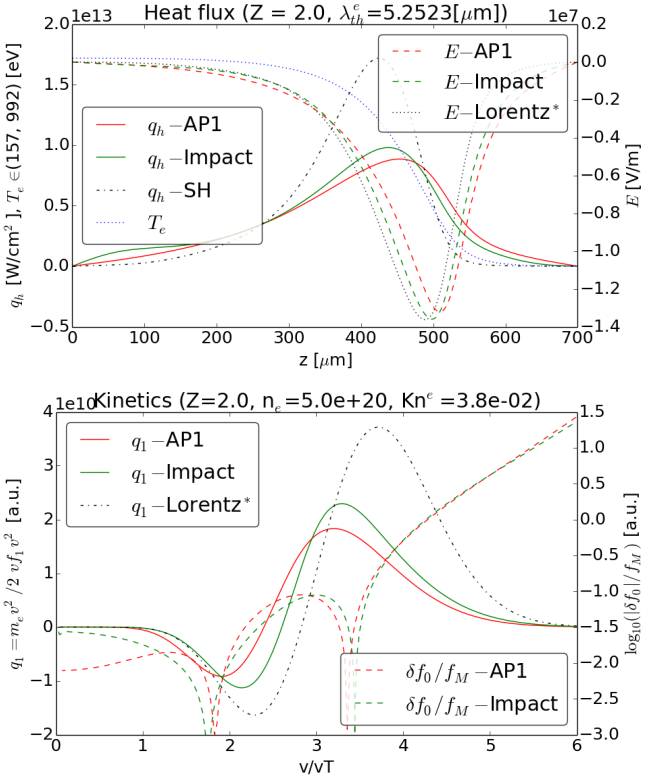

FIG. 4. Snapshot 12 ps. Left: correct steady solution of heat flux. Right: correct comparison to kinetic profiles at point 437 μm by Impact. Velocity limit 4.0 v_{th}.

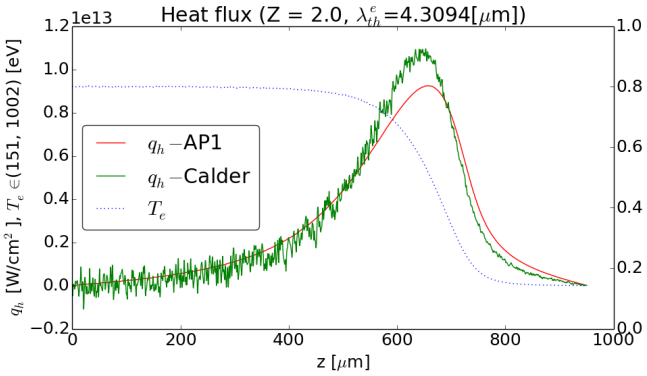

FIG. 5. Snapshot 11 ps. Left: correct steady solution of heat flux. Velocity limit 6.4 v_{th}.

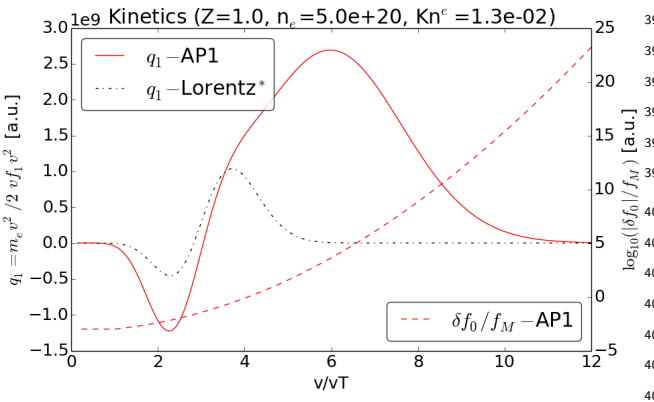

FIG. 6. Snapshot 12 ps. AP1 kinetic profiles at point 580 μm corresponding to a highly nonlocal nature of the heat flux FIG. 2 and is in a good agreement with [29]. Velocity $max(q_1)$ = 6.0 v_{th}. Velocity limit 9.0 v_{th}.

Impact and Calder codes in calculating the heat flow in the case where we have a large relative temperature variation. We consider the case of an initial temperature profile consisting of a ramp connecting two large hot and cold regions (baths). This has the advantages of allowing simple reflective boundary conditions and not requiring any external heating/cooling mechanisms that would also need to be carefully calibrated between codes.

The hot and cold baths had temperatures of T 0 and 0.15T 0 ; these were connected by a cubic ramp given by

$$\tanh(z)$$

For these simulations the electron density, Coulomb logarithm and ionisation were all kept constant and uniform.

Aladin and Impact simulations showed an evolution of the heat flow from the local (due to initialising as a Maxwellian) to the nonlocal, with a reduced peak, over an initial transient phase (over which the temperature ramp flattened some- what). The transient phase was considered over when the ratio of the VFP heat flow to the expected local heat flow stopped decreasing. After the transient phase this ratio begins to slowly increase as the thermal conduction flattens the temperature ramp and the ratio of the scalelength to mfp increases (i.e. the thermal transport slowly becomes more local). We then took the temperature profile from Aladin/Impact/Calder and used our AP1 implementation to calculate the heat flow they would predict given this profile.

2. *Hohlraum problem*

While comparisons between the AP1 model and VFP codes have previously been performed 8,45 , none have included spatially-inhomogeneous ionisation. As inertial fusion experiments involve steep ionisation and density gradients (for example, at the interface between the helium gas-fill and the ablated gold plasma), it is critical that the AP1 model be tested in such an environment. For evaluating this, the IMPACT [28] VFP code was used due to its ability to simulate inhomogeneous ionisation profiles.

We performed a HYDRA simulation in 1D spherical geometry of a laser-heated gadolinium hohlraum containing a typical helium gas-fill. A leak source was implemented with an area equal to the laser entrance hole to reproduce the energy balance. Electron temperature T_e, electron density n_e and ionisation Z profiles (shown in FIG. 8) at 20 nanoseconds were extracted and used as the initial conditions (along with the assumption that the electron distribution function is initially Maxwellian everywhere) for the IMPACT simulation (which was performed instead in planar geometry). At this point very steep gradients in all three variables were set up with a change from T_e = 2.5 keV, n_e = 5×10^{20} cm^3, Z = 2 to T_e = 0.3 keV, n_e = 5×10^{21} cm^3 , Z = 39 across approximately 100 μm at the helium-gadolinium interface. Spline interpolation was used to increase the spatial resolution near the steep interface for the IMPACT simulations, helping both numerical stability and runtime due to needing a reduced number of nonlinear iterations. For simplicity, the Coulomb logarithm was treated as a constant $\ln\Lambda_{ei} = \ln\Lambda_{ee} = 2.1484$. Note that in reality the plasma is only strongly coupled in the colder region of the gadolinium bubble beyond ∼1.7 mm and $\ln\Lambda_{ei} \approx 8$ up to ∼1.6 mm in the hotter corona. Reflective boundary conditions were used here as in the previous section and IMPACT used a timestep of 1.334 fs. The n_e and Z profiles did not evolve in the IMPACT simulation due to the treatment of the electric field discussed in section II that ensures quasineutrality and the neglection of ion motion and ionisation models.

As with the VFP simulations in the previous section, there is an initial transient phase where the IMPACT heat flux gradually reduces from the Braginskii prediction as the distribution function rapidly moves away from Maxwellian. Once again this transient phase is considered to be over when the ratio of the peak heat flow to the Braginskii prediction stops reducing. This ratio is not observed to change by more than 5% after the first 5 ps of our 15.7 ps simulation. Therefore, we conclude that it safe to assume the transient phase is over after 5 ps, at which point the temperature front has advanced by approximately 8 μm leading to a maximum temperature change of 41% as shown in FIG. 8. In comparing the IMPACT, AP1, and SNB heat flow profiles we encountered an important subtlety concerning the implementation of the model. A recent SNB model with separate electron ion and electron-electron collision frequencies provides a very good prediction of the preheat into the hohlraum, the peak heat flow to within 16% and an improved estimate of the thermal conduction in the gas-fill region, the latter is still too large by a factor of ∼2. This discrepancy could potentially lead to an overestimate of hohlraum

temperatures and thus cause issues similar to those arising with using an overly restrictive flux limiter.

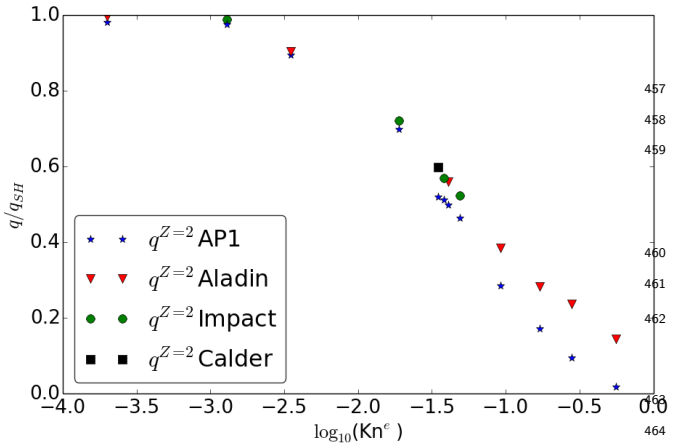

FIG. 7. Simulation results for the case $Z = 2$ computed by AP1/Aladin/Impact/Calder. Every point corresponds to the maximum heat flux in a "tanh" temperature simulation, which can be characterized by Kn. The range of $\log_{10}(\mathrm{Kn}) \in (0, -4)$ can be expressed as equivalent to the electron density approximate range $\mathrm{n}_e \in (1e19, 3.5e22)$ of the 50 μm slope tanh case. In the case of $\mathrm{Kn} = 0.56$, $q_{Aladin}/q_{AP1} \approx 7.9$.

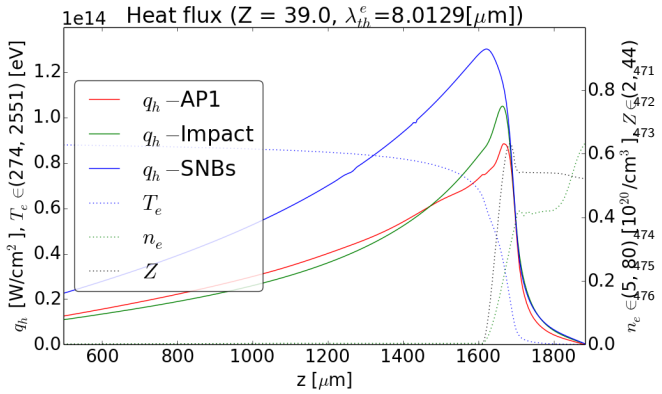

FIG. 8.

- Multiple runs analyzing the performance of AP1 with respect to Aladin/Impact/Calder along wide range of Kn^e shown in FIG. 7.

- Realistic hydro simulation setting provided by HYDRA, a comparison between AP1, Impact, and SNB shown in FIG. 8.

- Comment on and summarize the velocity limits for all figs.

V. CONCLUSIONS

- The most important point is that we introduce a collision operator, which is coherent with the full FP, i.e. no extra dependence on Z.

- Touch pros/contras of linearized FP in Aladin and Impact vs AWBS

- Raise discussion about what is the weakest point of AP1 for high Kns: the velocity limit or phenomenological Maxwellization?

- Summarize useful outcomes related to plasma physics as the tendency of the velocity maximum in q_1 with respect to Z and Kn^e.

- Emphasize the good results of Aladin (compared to Impact) and also outstanding results of Calder while being PIC.

ACKNOWLEDGMENTS

[1] R. S. Cohen, L. Spitzer, Jr., P. M. Routly, The electrical conductivity of an ionized gas, Phys. Rev. 80 (1950) 230–238.

[2] J. H. Jeans, Astronomy and Cosmogony, Cambridge University Press, London, 1929.

[3] S. Chandrasekhar, Stochastic problems in physics and astronomy, Rev. Mod. Phys. 15 (1943) 1.

[4] M. Planck, Über einen Satz der statistischen Dynamik und seine Erweiterung in der Quantentheorie, Sitzungsber. Preuss. Akad. Wiss. 24 (1917) 324–341.

[5] L. Spitzer, Jr. and R. Härm, Transport phenomena in a completely ionized gas, Phys. Rev. 89 (1953) 977.

[6] M. N. Rosenbluth, W. M. MacDonald, D. L. Judd, Fokker-planck equation for an inverse-square force, Phys. Rev. 107 (1957) 1.

[7] A. R. Bell, R. G. Evans, D. J. Nicholas, Phys. Rev. Lett. 46 (1981) 243.

[8] J. P. Matte, J. Virmont, Electron heat transport down steep temperature gradients, Phys. Rev. Lett. 49 (1982) 1936–1939.

[9] S. I. Braginskii, Transport processes in a plasma, Reviews of Plasma Physics 1 (1965) 205.

[10] C. K. Birdsall, A. B. Langdon, Plasma Physics Via Computer Simulation, McGraw-Hill, New York, 1985.

[11] S. M. Guerin, A. R. Bell, J. R. Davies, M. G. Haines, One-dimensional particle simulations of fast electron transport in solid targets, Plasma Phys. Contr. F. 41 (1999) 285.

[12] F. Perez, L. Gremillet, A. Decoster, M. Drouin, E. Lefebvre, Improved modeling of relativistic collisions and collisional ionization in particle-in-cell codes, Phys. Plasmas 19 (2012) 083104.

[13] J. R. Albritton, E. A. Williams, I. B. Bernstein, K. P. Swartz, Nonlocal electron heat transport by not quite maxwell-boltzmann distributions, Phys. Rev. Lett. 57 (1986) 1887–1890.

[14] L. Landau, Kinetic equation for the coulomb effect, Phys. Z. Sowjetunion 10 (1936) 154.

[15] N. J. Fish, Theory of current drive in plasmas, Rev. Mod. Phys. 59 (1987) 175.

[16] D. D. Sorbo, J.-L. Feugeas, P. Nicolai, M. Olazabal-Loume, B. Dubroca, S. Guisset, M. Touati, V. Tikhonchuk, Reduced entropic model for studies of multidimensional nonlocal transport in high-energy-density plasmas, Phys. Plasmas 22 (2015) 082706.

[17] D. D. Sorbo, J.-L. Feugeas, P. Nicolai, M. Olazabal-Loume, B. Dubroca, V. Tikhonchuk, Extension of a reduced entropic model of electron transport to magnetized nonlocal regimes of high-energy-density plasmas, Laser Part. Beams 34 (2016) 412–425.

[18] P. Bhatnagar, E. Gross, M. Krook, A Model for Collision Processes in Gases. I. Small Amplitude Processes in Charged and Neutral One-Component Systems, Phys. Rev. 94 (1954) 511–525.

[19] H. A. Lorentz, The motion of electrons in metallic bodies, in: Proceedings of the Royal Netherlands Academy of Arts and Sciences, Amsterdam, Vol. 7, 1905, pp. 438–453.

[20] I. P. Shkarofsky, T. W. Johnston, M. P. Bachynskii, The particle Kinetics of Plasmas, Addison-Wesley, Reading, 1966.

[21] C. L. Longmire, Elementary Plasma Physics, Intersci. Pub., 1963.

[22] E. M. Epperlein, R. W. Short, A practical nonlocal model for electron heat transport in laser plasmas, Phys. Fluids B 3 (1991) 3092–3098.

[23] R. C. Malone, R. L. McCroy, R. L. Morse, Phys. Rev. Lett. 34 (1975) 721.

[24] D. G. Colombant, W. M. Manheimer, M. Busquet, Test of models for electron transport in laser produced plasmas, Phys. Plasmas 12 (2005) 072702.

[25] J. F. Luciani, P. Mora, J. Virmont, Nonlocal heat transport due to steep temeperature gradients, Phys. Rev. Lett. 51 (1983) 1664–1667.

[26] A. V. Brantov, V. Y. Bychenkov, V. T. Tikhonchuk, Nonlocal electron transport in laser heated plasmas, Phys. Plasmas 5 (1998) 2742–2753.

[27] G. Schurtz, P. Nicolai, M. Busquet, A nonlocal electron conduction model for multidimensional radiation hydrodynamics codes, Phys. Plasmas 4238 (2000) 7.

[28] R. J. Kingham, A. R. Bell, An implicit vlasovfokker-planck code to model non-local electron transport in 2-d with magnetic fields, J. Comput. Phys. 194 (194) (2004) 1–34.

[29] M. Sherlock, J. P. Brodrick, C. P. Ridgers, A comparison of non-local electron transport models for laser-plasmas relevant to inertial confienement fusion, Phys. Plasmas 24 (2017) 082706.

[30] A. Marocchino and M. Tzoufras and S. Atzeni and A. Schiavi and Ph. Nicolai and J. Mallet and V. Tikhonchuk and J.-L. Feugeas, Comparison for non-local hydrodynamic thermal conduction models, Phys. Plasmas 20 (2013) 022702.

[31] J. P. Brodrick, R. J. Kingham, M. M. Marinak, M. V. Patel, A. V. Chankin, J. T. Omotani, M. V. Umansky, D. D. Sorbo, B. Dudson, J. T. Parker, G. D. Kerbel, M. Sherlock, C. P. Ridgers, Testing nonlocal models of electron thermal conduction for magnetic and inertial confinement fusion applications, Phys. Plasmas 24 (2017) 092309.